Geophys. J. Int. (2002) **149,** 524–533

Are buoyancy forces important during the formation of rifted margins?

Mark Davis[1] and Nick Kusznir[2]

[1] *Shell International, Carel van Bylandtlaan* 23, *Postbus* 663, 2501 *CR, The Hague, The Netherlands. E-mail: m.j.davis@sepiv.shell.com*
[2] *Department of Earth Sciences, University of Liverpool,* PO Box 147, *Liverpool,* L69 3BX, *UK. E-mail: sr11@liverpool.ac.uk*

Accepted 27 November 2001. Received 16 November 2001; in original form 16 November 1999

SUMMARY

Profiles of crustal thickness across rifted continental margins are examined in an attempt to understand the key observations and controlling parameters. Crustal stretching factor profiles from rifted continental margins supplemented by isochron data for early seafloor spreading have been used to determine a correlation between strain-rate ($\dot{\varepsilon}$) and stretching factor (β). Despite the different methods, assumptions and data sources, our $\dot{\varepsilon}$–β relationship for rifted margins is consistent with that observed by Newman and White for intracontinental rift basins. The $\dot{\varepsilon}$–β relationship we derive is also consistent with the dynamic models of Newman and White which include thermorheological strain-hardening and strain-softening, but omit crustal buoyancy forces generated by lateral crustal thickness variations. Whilst crustal buoyancy forces are not included in the above dynamic models, the $\dot{\varepsilon}$–β data do not necessarily preclude their importance. Simple numerical models of buoyancy force evolution show that for the first ~30 Myr after rifting the thermally-derived buoyancy forces within the lithosphere that assist extension are larger than the crustal buoyancy forces that oppose extension. This 'rift push' force acts as a positive feedback mechanism, is of the order of 3×10^{12} N m^{-1} and dominates over the opposing crustal buoyancy forces immediately after rifting. It is therefore clear that the delocalising effects of the crustal buoyancy force are dominant over a restricted range of conditions, namely at low strain-rate and at long times after rifting. Histograms of the lateral pressure gradients derived from crustal thinning factors along rifted margins show a dominant peak at 0.05 ± 0.3 kPa m^{-1} and a significant secondary peak at 0.8 ± 0.3 kPa m^{-1}. The lower lateral pressure gradient peak corresponds to thinned parts of the continental crust which is adjacent to unstretched continental crust and may define the edge of a zone of thermal strain-softening. Independent observations show that narrow margins are associated with rapid strain-rates and are consistent with thermal strain-softening predicted by thermorheological models. However the dominant near-zero pressure gradient peak is consistent with the operation of crustal buoyancy force processes during rifting, which attempt to remove variations in crustal thickness.

Key words: continental margins, lithosphere, rifts, sedimentary basins.

1 INTRODUCTION

Despite the considerable success of kinematic models of continental lithosphere extension (e.g. McKenzie 1978; Wernicke 1985; Lister *et al.* 1991) they provide little insight into lithosphere dynamics which are controlled in part by the evolution of plate strength. The net strength of the lithosphere after deformation is a consequence of the contributions of several processes which either localise or delocalise (i.e. distribute) extension (Buck 1991). Processes that localise deformation include lithosphere (a) weakening in response to extension as elevated isotherms reduce the strength of lithospheric mantle which has a strongly temperature-dependent rheology. Such 'strain-softening' effects promote strain localisation and stress concentration into thinned lithosphere. In addition (b) thermal buoyancy forces generated as a consequence of lateral variations of temperature (hence density) within the lithosphere act as a positive feedback mechanism during rifting. Such 'rift push' buoyancy forces (e.g. Le Pichon & Alvarez 1984) have a time-dependent component. The magnitude, and hence significance, of thermal buoyancy forces is therefore a function of strain-rate. The two processes that act to delocalise extension are first, a 'strain-hardening' effect which promotes strain delocalisation as weak crust is replaced by strong mantle, thereby increasing the force required to continue deformation in the same location (Kusznir & Park 1987; Sonder & England 1989;

Newman & White 1997, 1999). Second, crustal thickness variations which are generated by lithospheric stretching generate horizontal buoyancy forces that oppose those that drive extension.

In this paper we take a joint observational and theoretical approach to investigate the relative importance of rheology and buoyancy processes during lithosphere extension. We examine profiles of crustal thickness across rifted continental margins to determine margin stretching factors and strain rates, and attempt to identify key similarities and controlling influences. A correlation (or relationship) between strain-rate ($\dot{\varepsilon}$) and stretching factor (β) is observed from rifted margins and compared with the models and data from Newman & White (1997, 1999) to assess the rôle of time-dependent strength changes in the lithosphere. Numerical modelling is used to predict the magnitude of both crustal buoyancy and thermal boundary forces and their development with time. In addition profiles of crustal thinning factor ($1 - 1/\beta$) profiles for rifted margins are used to produce profiles of the lateral variation in lower crustal pressure gradients in order to identify whether lithosphere deformation may be influenced by crustal buoyancy forces.

2 DETERMINATION OF STRETCHING FACTOR AND STRAIN-RATE

Width, extension and strain-rate have been computed for 24 profiles across rifted continental margins derived from seismic (wide-angle or normal incidence) or gravity modelling. 22 profiles are taken from Atlantic Ocean margins, 1 from the South China Sea and 1 from the Weddell Sea. In the case of volcanic margin profiles, the volcanic additions to crustal thickness through igneous underplating (as identified in the papers listed in Table 1) have been excluded and are not involved in the determination of stretching factors and extension. Intrusive bodies are not excluded from this analysis but are assumed to comprise only a small fraction of the gross rock volume. Crustal profiles are illustrated in Fig. 1 and the locations for the Atlantic Ocean examples are identified in Fig. 2. Table 1 details the data sources for this study. Figs 1 and 3(a) illustrate that the traditional view that margins may be classified as either 'narrow' (<75 km) or 'wide' (>250 km; e.g. Watts & Fairhead 1997) is over simplistic. Each profile runs from unstretched continental crust to the 'continent-ocean boundary' as interpreted by the authors indicated in Table 1.

2.1 Calculation of margin width, extension and stretching factor

The crustal stretching factor (β) profiling for each section has been determined from the present-day crustal thickness by assuming that the pre-rift crustal thickness is known and uniform. Pre-rift crustal thickness for each profile has been determined from the maximum value along its length and is typically ~32 km. The crustal stretching factor (β) is given by eq. (1). Table 2 provides a listing of the terms (and their numerical values) in the equations throughout this paper.

$$\beta = \frac{t_0}{t_c} \tag{1}$$

It is useful to define the crustal thinning factor (γ), which is complementary to the crustal stretching factor (β) and given by eq. (2):

$$\gamma = 1 - \frac{1}{\beta} \tag{2}$$

Table 1. Data sources for the crustal thinning profile used in this study (see also Fig. 2). Crustal thickness profiles are derived from seismic reflection, seismic refraction and/or gravity studies.

Profile number	Area	Reference
6	LASE	Keen *et al.* (1986)
	Georges Bank	Swift *et al.* (1987)
19	Gabon	Watts & Stewart (1998)
10	Makassar	Cloke *et al.* (1999)
11	Brazil	Chang *et al.* (1992)
	South China Sea	Davis (1999)
7, 8	Carolina	Klitgord *et al.* (1988)
3a & b	Orphan & Porcupine	Bassi *et al.* (1993)
4a & b	Flemish Cap & Goban Spur	Bassi *et al.* (1993)
5a & b	Newfoundland & Galicia	Bassi *et al.* (1993)
	Nova Scotia	Keen & Potter (1995)
16, 17	Hatton and Edoras	Barton & White (1997)
12	Weddell Sea	Hubscher *et al.* (1996)
1, 2	Labrador	Chian *et al.* (1995)
13	Lofoten	Kodaira *et al.* (1994)
15, 16	Møre and Vøring	Skogseid & Eldholm (1995)
9	Gulf of Lions	Bessis (1986)

The distance from unstretched crust to the conventional 'continent-ocean boundary' defines the margin width (W). We have assumed that the ocean-continent transition is sharp and as defined in the source references of Table 1. Whilst we use a single location for the 'continent–ocean boundary' in this work, we acknowledge that much recent work demonstrates that sometimes there may be no unique location of this boundary because a transitional zone of continental mantle is probably exhumed before the onset of seafloor spreading (e.g. Pickup *et al.* 1996; Manatschal & Bernoulli 1999; Whitmarsh *et al.* 2001; Davis 1999).

Table 2. Parameters used in this study.

Symbol	Quantity	Value	Units
β	stretching factor		—
γ	thinning factor		—
Pe	Peclet number		—
m, n, w	derived constants		—
C	empirically-derived constant		—
z	depth		km
WD	water depth		km
W	margin width		km
E	margin extension		km
t_c	crustal thickness		km
t_0	initial crustal thickness	30	km
a	lithosphere thickness	125	km
l	straining width		km
P	pressure		Pa
g	acceleration due to gravity	9.81	m s^{-2}
u_x	initial seafloor spreading rate		m s^{-1}
ρ	density		kg m^{-3}
ρ_m	mantle density	3330	kg m^{-3}
ρ_c	crustal density	2800	kg m^{-3}
ρ_w	water density	1030	kg m^{-3}
F	buoyancy force		N m^{-1}
t	time		Ma
$\dot{\varepsilon}$	horizontal strain-rate		s^{-1}
τ_c	conduction thermal time constant		Ma
τ_a	advection thermal time constant	62.8	Ma
k	thermal conductivity	2.8	W m^{-1} K^{-1}
κ	thermal diffusivity	6×10^{-7}	m^2 s^{-1}

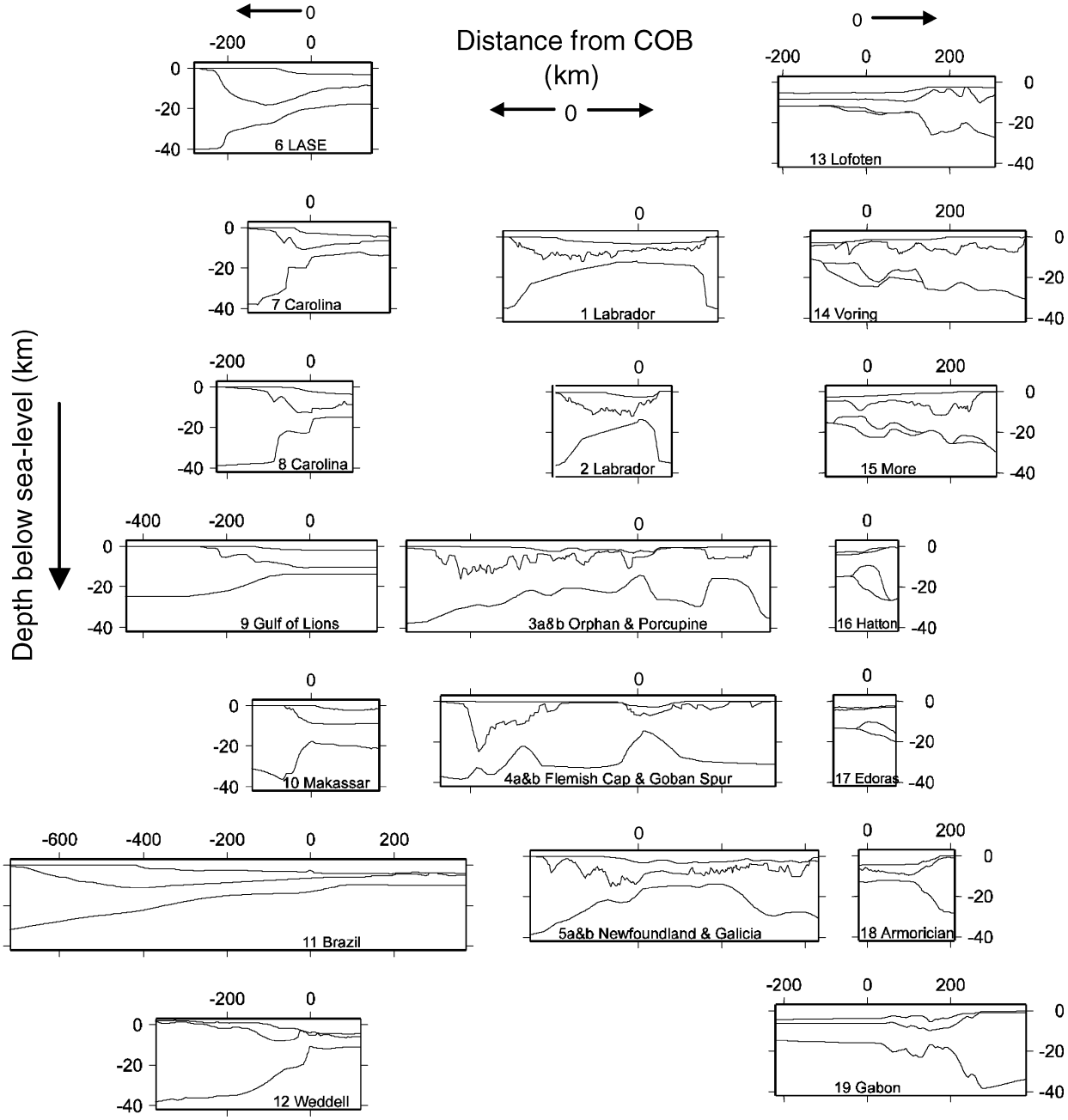

Figure 1. Cross-sections illustrating crustal thinning profiles at rifted margins used in this study (see Fig. 2 for their locations). Solid lines from top to bottom indicate the seabed, top basement, Moho and (where present) the base of crustal magmatic underplating. These profiles are derived from wide-angle, gravity or normal incidence studies (see Table 1 for data sources). All profiles are plotted with the same horizontal and vertical axis scaling and are centred on the continent-ocean boundary. Numbers on vertical and horizontal axes indicate depth and distance respectively in kilometres.

The total extension (E) associated with each crustal thinning profile may be calculated by integrating the thinning factor (γ) along the width of the margin, as given by eq. (3).

$$E = \int_0^W \left[1 - \frac{1}{\beta}\right] dx = \int_0^W \gamma \, dx \tag{3}$$

We define the mean stretching factor ($\bar{\beta}$, eq. 4) to be:

$$\bar{\beta} = \frac{1}{1 - E/W} \tag{4}$$

2.2 Calculation of margin strain-rate ($\dot{\varepsilon}$)

The crustal thinning profiles described above are combined with temporal data extracted from initial post-breakup seafloor spreading rates (u_x) to determine spatially averaged lithospheric strain-rates as defined in England (1983) and defined below in eq. (5). After England (1983), the horizontal strain-rate is:

$$\dot{\varepsilon} = \frac{u_x}{W} \tag{5}$$

Strain-rates calculated using eq. (5) are spatially averaged and are dependent on the horizontal length-scale over which straining is

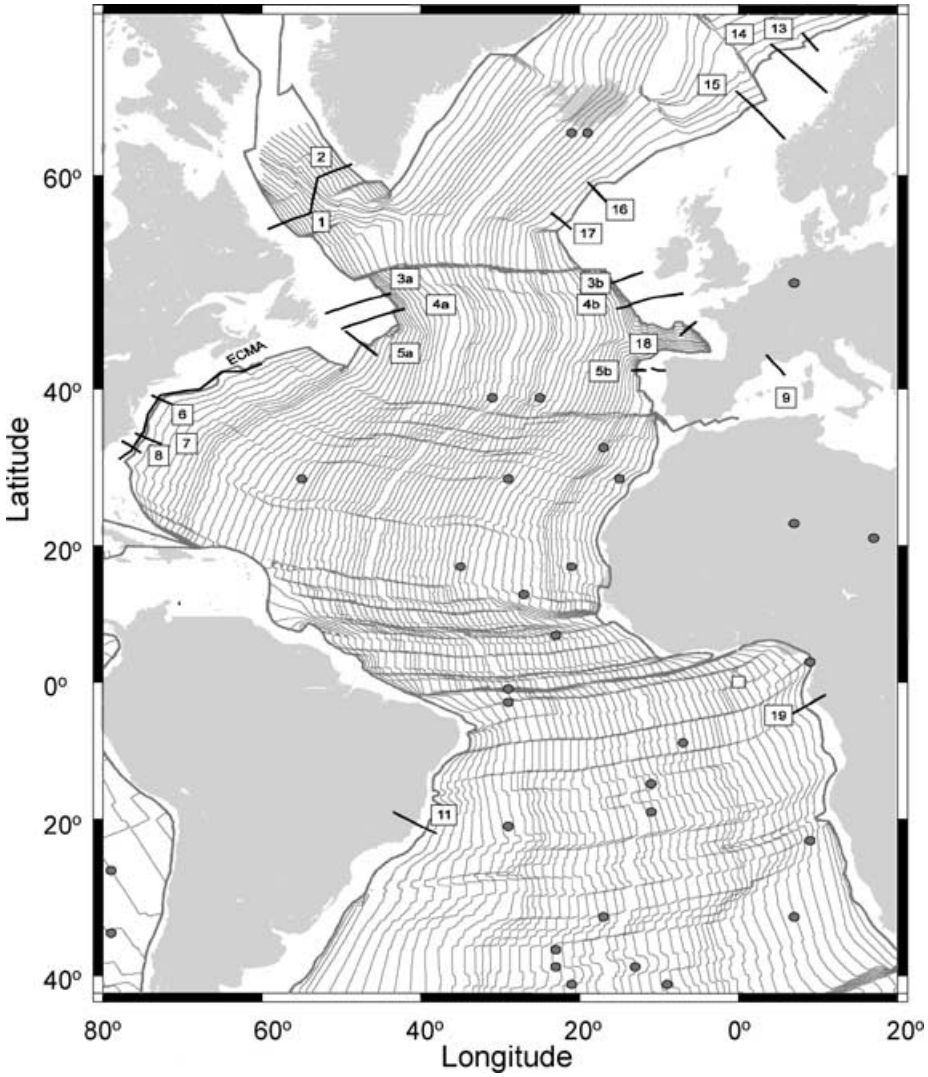

Figure 2. Distribution of margins studied in the Atlantic Ocean area. The numbers identify the crustal profiles and their data source (Table 2) illustrated in Fig. 1. The oceanic crust age is contoured at 5 Ma intervals from the data set of Mueller *et al.* (1997). Mantle plumes (from Nataf & Ricard 1996) are represented by dots.

assumed to occur (i.e. margin width, W) and the continental separation velocity (u_x). In the calculations that follow we assume that the initial (half-) rate of seafloor spreading is a proxy for the velocity of continental separation during the final stage of rifting. The strain-rate may be overestimated if the velocity during the latest rifting phase is less than that of initial seafloor spreading. Alternatively, it might be underestimated if only a fraction of the whole width of the rifted continental margin is involved in the breakup event. A reduction in the width over which breakup-related straining is assumed to occur increases the calculated mean strain-rates and stretching factors. As discussed above, an additional uncertainty associated with the definition of margin 'width' exists because there is a possibility of presence of a region of transitional crust between unequivocal continental and oceanic crust. Vertical strain-rates are derived from the calculated horizontal strain-rates assuming conservation of mass.

Figs 3(a) and (b) illustrates the observed relationship between seafloor spreading rate (Mueller *et al.* 1997 for the Atlantic Ocean and Weddell Sea; Briais *et al.* 1993 for the South China Sea) and margin width and extension data for regions as detailed in Table 1. Figs 3(a) and (b) show that highly extended margins (e.g. the Orphan margin) are associated with slow initial seafloor spreading rates, and vice versa (e.g. the Carolina margin).

Horizontal strain-rate is plotted against margin width and extension in Figs 3(c) –(e) and suggest that the lithospheric strain-rate is an important parameter in the evolution of rifted continental margins, although we recognise that strain rate and margin width are not independent, and that some inherent correlation exists between these two parameters. Peclet number vs margin extension is shown in Fig. 3(f).

2.3 Relationship between strain-rate and stretching factor

The mean stretching factor and strain-rate ($\dot{\varepsilon}$-β) estimates at rifted margins from this study are illustrated in Fig. 4(a) and are compared in Fig. 4(b) with those of Newman & White (1997) for intracontinental rift basins. Errors associated with our data are of the order of $\Delta\beta = 0.3$ and half an order-of-magnitude for strain-rate. We highlight that the data sets appear to be compatible and continuous despite different analytical methods spreading-rate derived strain rate in this study vs 1-D inversion of subsidence data in Newman

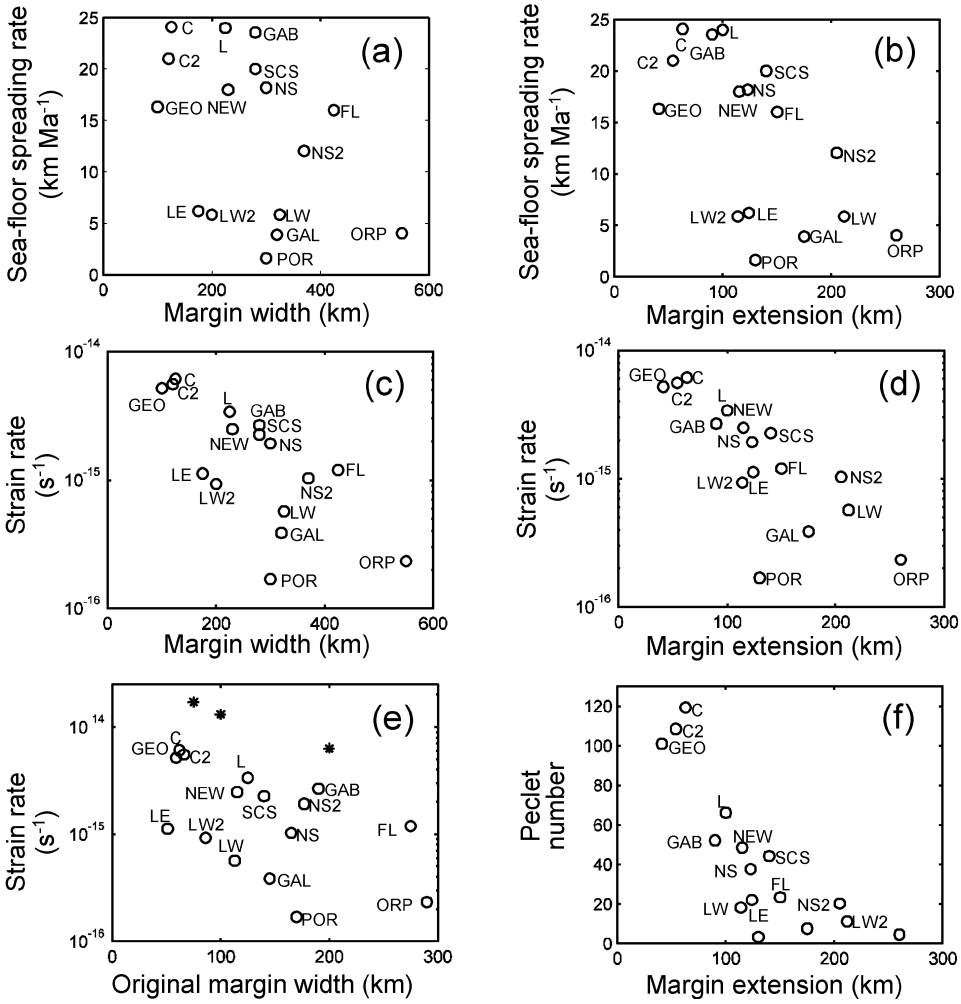

Figure 3. (a) Initial half-rate of seafloor spreading vs margin width. (b) Initial seafloor spreading rate vs maximum margin extension. (c) Pre-breakup strain-rate plotted against margin width. (d) Pre-breakup strain-rate against margin extension. (e) Strain-rate vs original margin width. Model results from England (1983) are also included as asterisks. (f) Peclet number vs margin extension. Letter code for margins: C = Carolina, C2 = Carolina (alternative), L = LASE, SCS = South China Sea, FL = Flemish Cap, ORP = Orphan, POR = Porcupine Basin, GAL = Galicia margin, LW = Labrador West, LW2 = Labrador West (alternative), LE = Labrador East, NS = Nova Scotia, NS2 = Nova Scotia (alternative), NEW = Newfoundland margin, GEO = St Georges Bank, GAB = Gabon. See Table 2 for data sources and references.

& White 1999) and data sources (rifted margins in this study vs intracontinental rift basins with stretching almost exclusively less than $\beta = 1.5$ in Newman & White). Fig. 4(b) also illustrates the model predictions of Newman & White (1999) whose model incorporates thermorheological strain-hardening and strain-softening but omits crustal buoyancy forces. Such model predictions appear to be consistent with the combined observations for rift margin and intracontinental rift basins.

A dimensionless number which appears to usefully mark the boundary between sedimentary basins and rifted margin is the Peclet number (Pe, eq. 6), which is given by:

$$\mathrm{Pe} = \frac{\tau_c}{\tau_a} = \frac{a^2}{\kappa}\dot{\varepsilon} \tag{6}$$

A critical Peclet number appears to separate the data from sedimentary basins (from Newman & White 1997) which have low Peclet numbers (Pe < 20) from those from rifted continental margins (where Pe is mostly >20). Fig. 4(b) suggests that the stretching factor might become independent of strain-rate above a critical Peclet number of Pe ~ 20 (strain-rate 10^{-15} s^{-1}).

3 BUOYANCY FORCES DURING RIFTING

The relationships derived from this study and that of Newman & White (1999) appear to be consistent with the latter authors' dynamic modelling predictions which include the influence of thermorheological strain-hardening and strain-softening, but deliberately omit crustal buoyancy forces. Whilst this may suggest that crustal buoyancy forces are not relevant, we suggest that crustal buoyancy may be responsible for much of the scatter, and the results do not necessarily preclude their significance.

The response of the lithosphere to stretching is illustrated in Figs 5(a) and (b). Immediately after stretching two opposing buoyancy forces are generated: (i) a crustal buoyancy force which is generated by the juxtaposition of thinned (and subsided) continental crust against unstretched crust, and; (ii) a thermal buoyancy (or 'rift-push') force generated by the juxtaposition of hot (thermally expanded) low-density rocks against cold rocks (Fig. 5b). Whilst thermal expansion-related density changes are very small (for a 500 K temperature difference such variations are more than one order-of-magnitude smaller than the density contrast at the Moho),

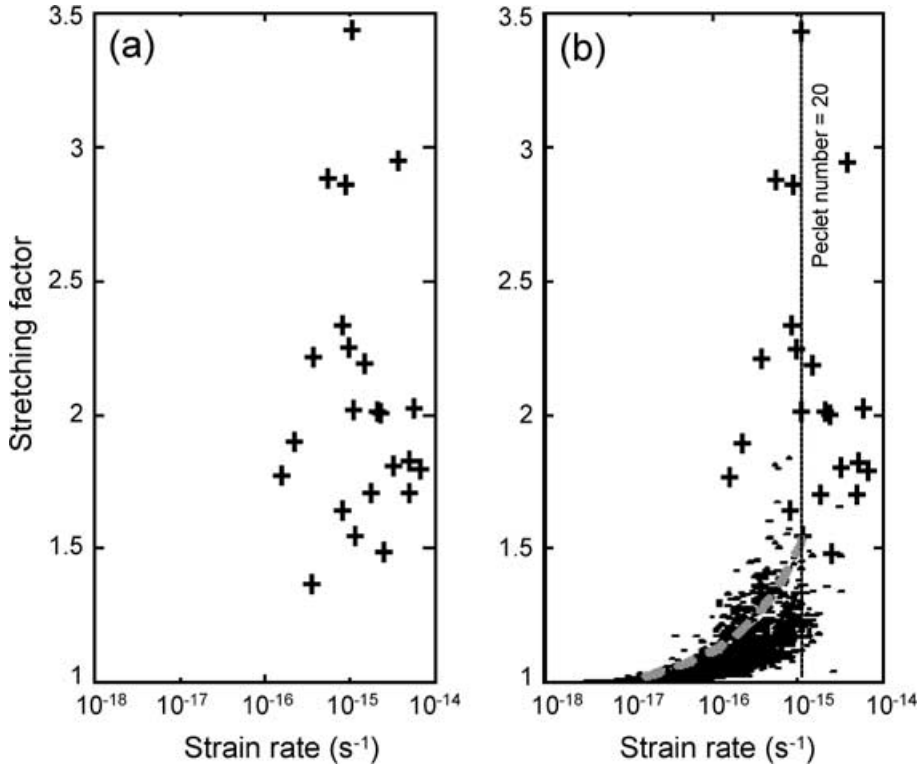

Figure 4. (a) Strain-rates and stretching factors derived from rifted continental margins (this study), (b) Strain-rates and stretching factors derived from rifted continental margins (crosses) compared with strain-rate and stretching factors for sedimentary basins (Newman & White 1997, 1999). Despite the very different methods used in their determination, there is a clear continuity between sedimentary basins and rifted continental margins. The predictions of the model from Newman & White (1999) which includes thermorheological strain-hardening and strain-softening but omits crustal buoyancy forces is shown by the dashed line. Almost all the data from sedimentary basins have Peclet numbers (Pe) < 20.

the contribution when integrated over the lithosphere is considerable. The time-dependent thermal buoyancy force which is oppositely directed to the crustal buoyancy force, may be the dominant intraplate force generated for several tens of millions of years after rifting.

3.1 Development of a numerical expression for net buoyancy force

Computation of the magnitude of the total thermal and crustal buoyancy force as a function of time was performed with a 1-D numerical model which incorporates the thermal, density and subsidence history of the lithosphere and is illustrated in Fig. 6. It is not possible to develop a simple analytical solution to describe the evolution of the net buoyancy force but this may be determined easily using numerical computation. In our 1-D model, instantaneous uniform stretching is applied to a lithosphere comprising of crust and mantle, each with temperature-dependent density. The top and base temperature boundary conditions are 0 and 1333 °C respectively and radiogenic contributions are ignored. Density is assumed to be controlled by temperature (eq. 7).

$$\rho = \rho_0(1 - \alpha T) \tag{7}$$

As time elapses after stretching the model predicts the temperature, density, pressure and water-loaded subsidence (Figs 5a and 6a) through the 1-D solution of the governing equation for the conservation of heat (eq. 8). For simplicity of illustration the basin generated in Fig. 5 is air-filled.

$$\frac{\partial T}{\partial t} = \kappa \nabla^2 T \tag{8}$$

By definition, pressure is given by eq. (9):

$$P = \int_0^\infty g\rho(z)\, dz \tag{9}$$

The lithosphere is assumed to be in local isostasy at all times. The subsidence of the lithosphere surface required to satisfy this condition is computed numerically.

The net buoyancy force is the integral with depth of the lateral pressure difference (Fig. 6b) between the reference and stretched column and is illustrated as a function of time and stretching factor (β) in Fig. 6(c). The buoyancy force at any depth is derived numerically (eq. 10). Depth z is measured with respect to sea level.

$$F_{\text{net}} = \int_0^z \Delta P\, dz \tag{10}$$

A positive buoyancy force corresponds to relative horizontal compression within the stretched lithosphere and a negative value to relative horizontal tension. Fig. 6(c) illustrates that the total buoyancy force (F_{net}) is a strong function of time and stretching factor (β). In keeping with Buck (1991), the thermal buoyancy force is larger than the crustal buoyancy force at rifting for the typical ranges of values for lithosphere and crustal thermal properties. The thermal buoyancy force has a typical maximum value $\sim 3 \times 10^{12}$ N m^{-1} immediately after instantaneous stretching for a rifted continental margin with $\beta = 5$. The magnitude of this 'rift-push' force is

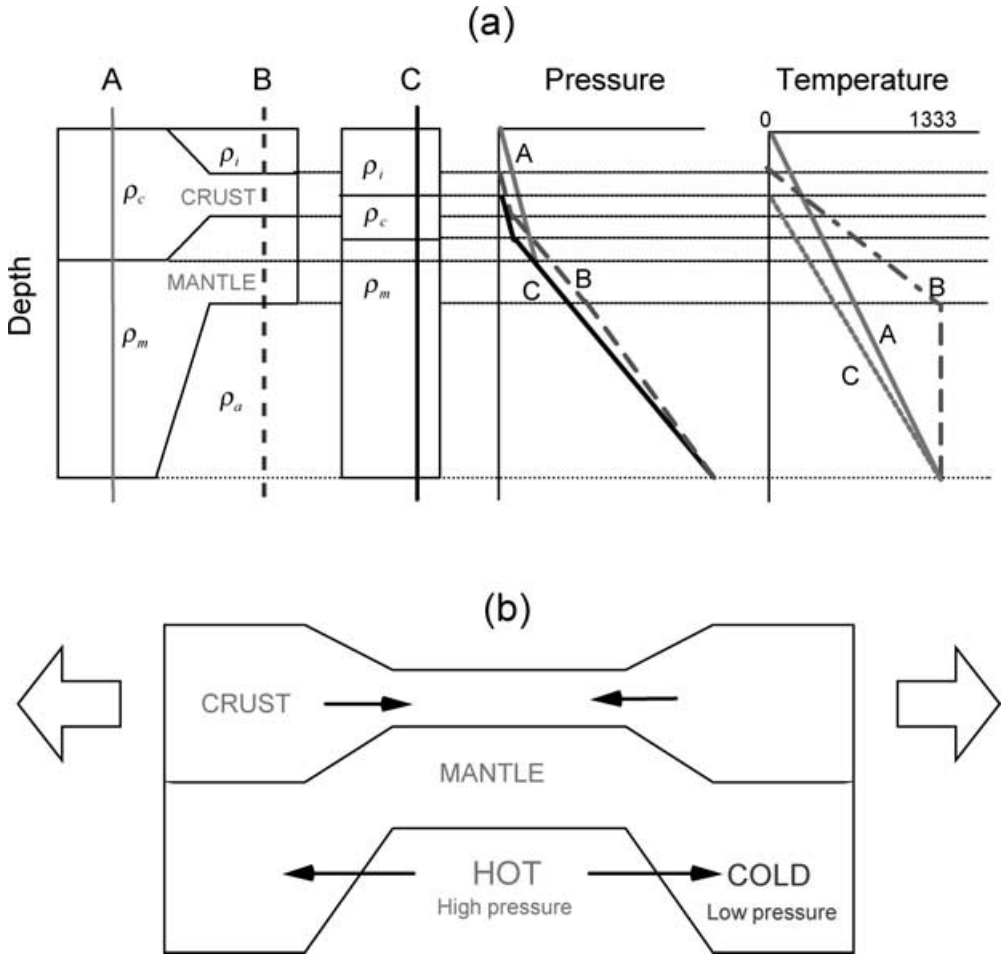

Figure 5. Schematic diagram illustrating the origins of the 'rift-push' force that assists the plate driving forces immediately after rifting and acts as a positive feedback mechanism that tends to localise rifting. (a) Schematic diagram illustrating pressure and temperature as a function of depth in: (A) unstretched continental lithosphere; (B) stretched lithosphere immediately after rifting; (C) final stretched lithosphere after thermal re-equilibration. (b) The 'rift-push' force acts in the opposite direction to the crustal buoyancy force.

comparable to other well recognized plate tectonic forces as described by Kusznir (1991) and summarised in Table 3. The most critical parameter controlling the influence of the thermal buoyancy force is the extensional strain rate. Clearly, the thermal buoyancy force is expected to be lower if the strain-rate is reduced. Figs 5(b) and 6(c) illustrates that the 'rift-push' force generated during rifting (e.g. Le Pichon & Alvarez 1984) acts outwards from the basin axis and throws thinned lithosphere into tension. Only as the lithosphere cools and after 30–50 Myr does the crustal buoyancy force dominate. The 'rift-push' force therefore acts as a positive feedback mechanism in the initial stages of rifting and immediately after rifting has a comparable magnitude to the ridge push force (Table 3). Whilst the 'rift-push' force has been noted in earlier work (e.g. Buck 1991), it is rarely discussed in detail. Further analysis of the crustal buoyancy force is presented below.

3.2 Analytical expression for the crustal buoyancy force

An analytical solution for the crustal buoyancy force is presented below for lithosphere in which the thermal anomaly generated by rifting has equilibrated. Crustal thickness variations are assumed to be compensated locally by Airy isostasy only and is therefore appropriate for lithosphere that has achieved steady-state after infinite time and with no contributions from Pratt isostasy. Unlike the numerical model presented above, in this analytical solution we ignore the dependence of crustal density on temperature.

Assuming Airy isostasy, change in water depth is controlled by crustal thickness changes eq. (11):

$$\Delta WD = \Delta t_c \left[\frac{\rho_m - \rho_c}{\rho_m - \rho_w} \right] \tag{11}$$

but:

$$\Delta t_c = t_0 \left[1 - \frac{1}{\beta} \right] = t_0 \gamma \tag{12}$$

hence t the water depth is:

$$\Delta WD = \Delta t_0 \gamma w \tag{13}$$

where

$$w = \left[\frac{\rho_m - \rho_c}{\rho_m - \rho_w} \right] \tag{14}$$

In order to calculate the lateral buoyancy force generated by Airy-isostatically compensated crustal thickness variations (Fig. 7), the integrals of the pressures in columns A and B are subtracted. The crustal buoyancy force (F_c) is therefore equal to the area stippled in

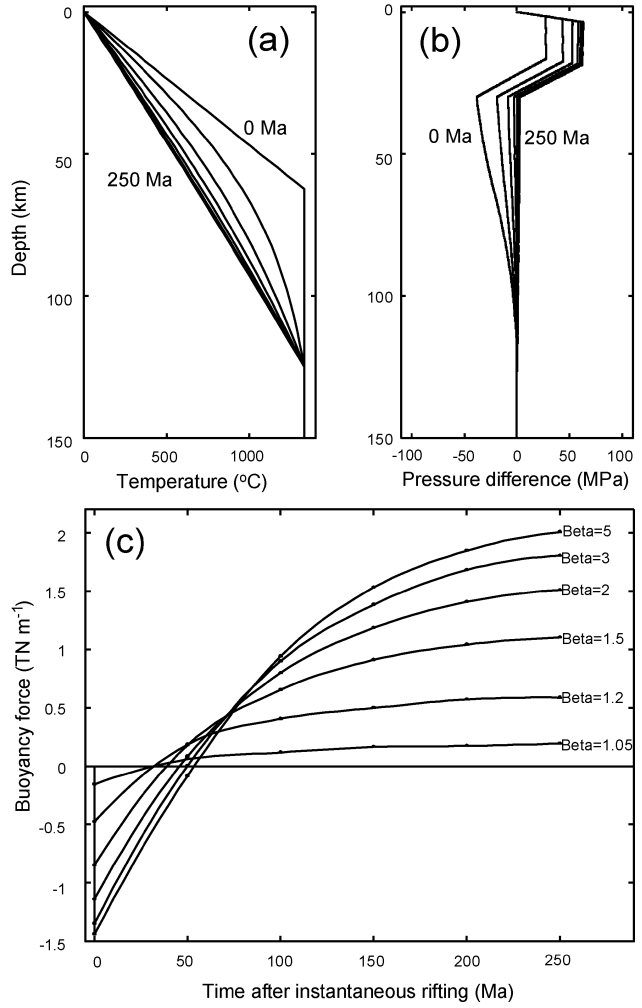

Figure 6. (a) Temperature and; (b) buoyancy force as a function of time for stretched continental lithosphere in local isostatic equilibrium, for a uniform stretching factor $\beta = 2$. No radiogenic heating is incorporated. (c) Magnitude of the total (net) buoyancy force as a function of time and stretching factor (β). Negative buoyancy forces act to enhance extension and positive buoyancy forces provide negative feedback. Note that immediately after instantaneous rifting the thermal contribution to the buoyancy force dominates.

Fig. 7(b). It may be shown that the crustal buoyancy force is given by:

$$\frac{F_c}{gt_0^2} = \frac{\gamma w \rho_w}{2} + (1-\gamma)\gamma w \rho_w + \frac{(1-\gamma)^2 \rho_c}{2} + \gamma(1-w) \times [(1-\gamma)\rho_c + \gamma w \rho_w] + \frac{\gamma^2(1-w^2)\rho_m}{2} - \rho_c \quad (15)$$

which after simplification becomes:

Table 3. Magnitudes of the principal tectonic forces within lithosphere plates, after Kusznir (1991). The magnitude of the 'rift-push' force is comparable to other well recognized tectonic forces.

Origin of force	Magnitude (TN m^{-1})
Ridge push	2–3
Subduction suction	0–3
Subduction slab pull	0–5
Plateau uplift	0–4
Continental margins	1–2
'Rift push' (this work)	0–3.5

$$F_c = gt_0^2(m\gamma^2 + n\gamma) \quad (16)$$

where

$$m = \frac{w^2}{2}(\rho_m - \rho_w) + w(\rho_c - \rho_m) + \frac{1}{2}(\rho_m - \rho_c) \quad (17)$$

$$n = w(\rho_w - \rho_c) \quad (18)$$

4 MOHO TOPOGRAPHY AND PRESSURE GRADIENTS AT RIFTED MARGINS

The pressure difference between two points at the same depth in adjacent columns of lithosphere is controlled by the density and thickness of the overlying materials (Fig. 7b). Assuming Airy isostasy, the lateral pressure gradient within stretched crust at any level is:

$$\frac{\partial P}{\partial x} = gt_0\left(\frac{\rho_m - \rho_c}{\rho_m - \rho_w}\right)(\rho_c - \rho_w)\frac{\partial \gamma}{\partial x} \quad (19)$$

Fig. 8(a) shows thinning (γ) factors as a function of distance from the 'continent-ocean boundary' from crustal thinning profiles illustrated in Figs 1 and 2. Fig. 8(b) shows a schematic interpretation of the observed pressure gradients shown in Fig. 8(a). Histograms of the lateral pressure gradients for narrow margins illustrated in Fig. 8(c) suggest that two prominent peaks are present and support the presence of the linear trends apparent in Fig. 8(a). Since fault-block topography generates considerable scatter in the observed pressure gradients, a Butterworth long wavelength pass filter (pass wavelength >25 km) has been applied to the data before binning. Figs 8(c) shows that there are pressure gradients peaks at 0.8 ± 0.3 kPa m^{-1} and 0.05 ± 0.3 kPa m^{-1}. It is remarkable that the distribution of lateral pressure gradients is not continuous but have two well-resolved peaks. The low pressure gradient of 0.05 ± 0.3 kPa m^{-1} corresponds to highly thinned continental crust, whilst the secondary (high) pressure gradient peak appears to be strongly associated with the boundary between stretched and unstretched crust (Figs 8c and d). We suggest that the peak at 0.8 ± 0.3 kPa m^{-1} reflects the initial strength of the (lower) crust at the start of rifting. The lower pressure gradient of 0.05 ± 0.3 kPa m^{-1} has two possible explanations, either: (a) crustal extension occurs until a critical low pressure gradient is reached after which strain is delocalised and occurs elsewhere, or; (b) the lower crust flows if the pressure gradient exceeds a critical limit. It is perhaps surprising that the limiting pressure gradient (and therefore implied strength?) is uniform given that the influence of temperature variations is expected to be profound in a system with temperature-dependent rheology.

In Figs 3(a) and (b) our data demonstrate that narrow rifted margins appear to be associated with fast initial seafloor spreading rates and rapid strain-rates. Such observations are consistent with lithospheric strain-softening as predicted by thermorheological models (e.g. Kusznir & Park 1987; Sonder & England 1989; Newman & White 1999). In contrast, wide margins appear to be associated with low strain-rates. This would imply that the thermorheological mechanism is the dominant control of strain localisation or delocalisation, and that crustal buoyancy forces are not important.

It is paradoxical however that the pressure gradient results show a broad region of low strength crustal material for wide margins which implies that crustal buoyancy may play an important role in levelling the thickness of rifted margin crust. Modelling of thermal and crustal buoyancy forces (this paper) show that at high strain rates, the

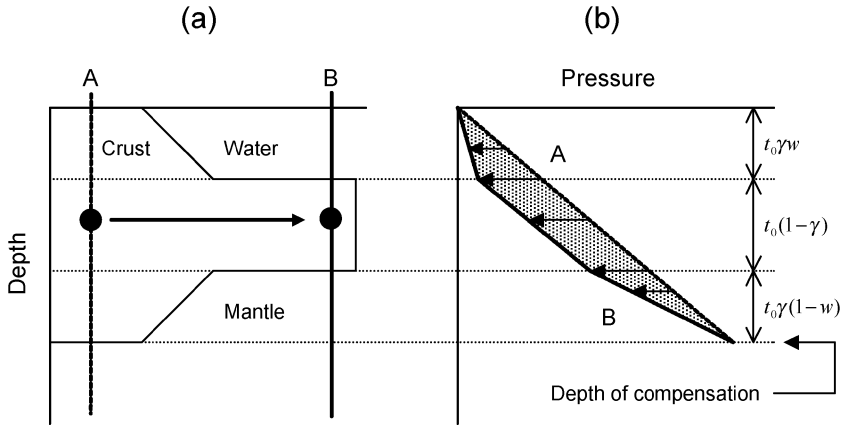

Figure 7. Schematic diagram to illustrate the calculation of lateral buoyancy force generated by water-loaded subsidence in response to crustal thinning assuming lithosphere thermal anomalies induced by rifting have equilibrated. (a) Crustal structure diagram with arrows indicating the direction of induced horizontal pressure gradient between two points within the crust marked by circles, and; (b) pressure as a function of depth. Location A marks unstretched continental crust and B marks stretched and subsided continental crust. Airy isostasy is assumed throughout.

localising effect of thermal buoyancy dominates over crustal buoyancy forces. However at low strain rates modelling indicates that crustal buoyancy forces may be more significant. Crustal buoyancy forces are therefore likely to be more important when strain-rates are low and result on in near-zero pressure gradients reflecting the removal of crustal thickness variations in response to the operation of buoyancy force processes during rifting.

5 CONCLUSIONS

Observations of strain-rate vs stretching factor at rifted margins are consistent with independent observations for intracontinental rifts. In addition both sets of observations (this work and Newman & White 1997) are consistent with predictions of dynamic models of the rheological response of the lithosphere to extension which neglect crustal buoyancy forces (Newman & White 1999). While crustal buoyancy forces are expected to enhance strain delocalisation, rift push buoyancy forces have the opposite influence. The 'rift push' buoyancy forces have been shown to dominate over crustal buoyancy forces for tens of millions of years after instantaneous rifting, and may explain why the rheological dynamic models which omit crustal buoyancy forces agree with observations (Newman & White 1997, 1999). Crustal buoyancy forces are therefore only likely to be important over a restricted range of conditions, namely where strain-rates are low. At low strain rates, crustal buoyancy forces may result in near-zero pressure gradients, as indicted by pressure gradient observations, reflecting the removal of crustal thickness variations.

ACKNOWLEDGMENTS

This paper has benefited from discussions with Mike Cheadle (Wyoming), Peter Styles (Keele) and Rob Newman (Cambridge).

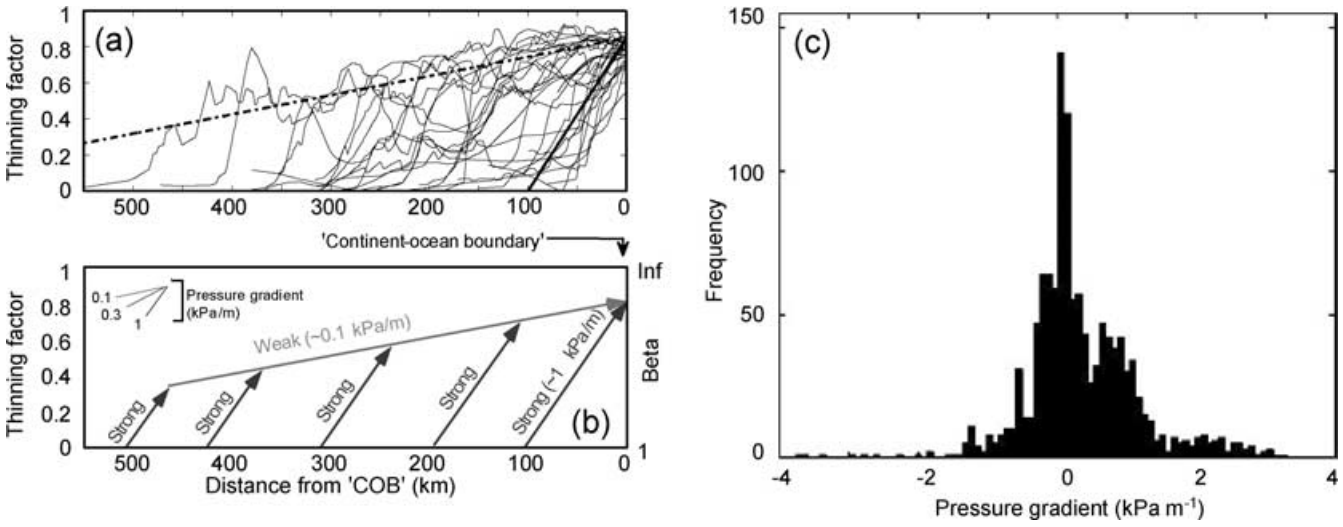

Figure 8. (a) Observed thinning factors as a function of distance from the continent-ocean boundary for studied rifted margins. Lines are superimposed corresponding to uniform lateral pressure gradients of ~1 kPa m^{-1} (steep gradient, solid) and ~0.1 kPa m^{-1} (shallow gradient, dashed). (b) Interpreted and simplified plot. All margins appear to be associated with a high lateral pressure gradient (~0.8 kPa m^{-1}, equivalent to a topographic gradient of ~3 per cent), bounding unstretched continental crust. Stretched crust is associated with a lower pressure gradient ~0.05 kPa m^{-1}. (c) Histogram of horizontal pressure gradients for narrow margins only, illustrating the importance of the higher pressure gradient (~0.8 kPa m^{-1}).

MJD gratefully acknowledges Nicky White (Cambridge) for allowing access to the data from Newman & White (1997, 1999). This work was carried out with support to MJD from a NERC studentship GT4/95/165/E. Critical reviews from Roger Buck, Dennis Harry and the editor are gratefully acknowledged.

REFERENCES

Barton, A.J. & White, R.S., 1997. Crustal structure of Edoras Bank continental margin and mantle thermal anomalies beneath the North Atlantic, *J. geophys. Res.,* **102,** 3109–3129.

Bassi, G., Keen, C.E. & Potter, P., 1993. Contrasting styles of rifting—models and examples from the eastern Canadian margin, *Tectonics,* **12,** 639–655.

Bessis, F., 1986. Some remarks on the study of subsidence of sedimentary basins: Application to the Gulf of Lions margin (Western Mediterranean), *Mar. Pet. Geol.,* **3,** 37–63.

Briais, A., Patriat, P. & Tapponier, P., 1993. Updated interpretation of magnetic anomalies and sea-floor spreading stages in the South China Sea: Implications for the Tertiary tectonics of Southeast Asia, *J. geophys. Res.,* **98,** 6299–6328.

Buck, W.R., 1991. Modes of continental lithospheric extension, *J. geophys. Res.,* **96,** 20 161–20 178.

Chang, H.K., Kowsmann, R.O., Figueiredo, A.M.F. & Bender, A.A., 1992. Tectonics and stratigraphy of the East Brazil rift system: An overview, *Tectonophysics,* **213,** 97–138.

Chian, D., Keen, C., Reid, I. & Louden, K., 1995. Evolution of non-volcanic rifted margins: New results from the conjugate margins of the Labrador Sea, *Geology,* **23,** 589–592.

Cloke, I.R., Milsom, J. & Blundell, D.J.B., 1999. Implications of gravity data from East Kalimantan and the Makassar Straits: a solution to the origin of the Makassar Straits?, *J. Asian Earth Sci.,* **17,** 61–78.

Davis, M.J., 1999. Lithospheric stretching at rifted continental margins, *PhD thesis,* University of Liverpool, Liverpool.

England, P., 1983. Constraints on extension in the continental lithosphere, *J. geophys. Res.,* **88,** 1145–1152.

Hubscher, C., Jokat, W. & Miller, H., 1996. Crustal structure of the Antartic continental margin in the eastern Weddell Sea, in *Weddell Sea tectonics and Gondwana break-up*, eds Storey, B., King, E. & Livermore, R., *Geol. Soc. Lond. Spec. Publ.,* London, **108,** 165–174.

Keen, C.E. & Potter, D.P., 1995. Formation and evolution of the Nova-Scotian rifted margin—evidence from deep seismic refraction data, *Tectonics,* **14,** 918–932.

Keen, C. *et al.*, 1986. Deep structure of the US East Coast passive margin from large aperture seismic experiments (LASE), *Mar. Pet. Geol.,* **3,** 234–242.

Klitgord, K., Hutchinson, D. & Schouten, H., 1988. US Atlantic continental margin: structural and tectonic framework, in *The Geology of North America,* eds Sheridan, R. & Grow, J., *Geol. Soc. Am.,* Colorado, **12,** 19–55.

Kodaira, S. *et al.*, 1994. Crustal structure of the Lofoten continental margin, off N Norway, by OBS refraction studies, *Geophys. J. Int.,* **121,** 907–924.

Kusznir, N.J., 1991. The distribution of stress with depth in the lithosphere: thermorheological and geodynamic constraints, *Phil. Trans. R. Soc. Lond.,* A., **337,** 95–110.

Kusznir, N.J. & Park, R.G., 1987. The extensional strength of the continental lithosphere: its dependence on continental gradient, and crustal composition and thickness, in *Continental Extension Tectonics,* eds Coward, M.P., Dewey, J.F. & Hancock, P.L., *Geol. Soc. Lond.,* London, **28,** 35–52.

Le Pichon, X. & Alvarez, F., 1984. From stretching to subduction in back-arc regions—dynamic considerations, *Tectonophysics,* **102,** 343–357.

Lister, G.S., Etheridge, M.A. & Symonds, P.A., 1991. Detachment models for the formation of passive continental margins, *Tectonics,* **10,** 1038–1064.

Manatschal, G. & Bernoulli, D., 1999. Architecture and tectonic evolution of nonvolcanic margins: Present-day Galicia and ancient Adria, *Tectonics,* **18,** 1099–1119.

McKenzie, D.P., 1978. Some remarks on the development of sedimentary basins, *Earth planet. Sci. Lett.,* **40,** 25–32.

Mueller, R.D., Roest, W.R., Royer, J.Y., Gahagan, L.M. & Sclater, J.G.S., 1997. Digital isochrons of the world's ocean floor, *J. geophys. Res.,* **102,** 3211–3214.

Nataf, H.C. & Ricard, Y., 1996. 3SMAC—An *a priori* tomographic model of the upper-mantle based on geophysical modelling, *Phys. Earth planet. Inter.,* **95,** 101–122.

Newman, R. & White, N.J., 1997. Rheology of the continental lithosphere inferred from sedimentary basins, *Nature,* **385,** 621–624.

Newman, R. & White, N.J., 1999. The dynamics of extensional sedimentary basins: constraints from subsidence inversion, *Phil. Trans. R. Soc. Lond.,* A., **357,** 805–834.

Pickup, S.L.B., Whitmarsh, R.B., Fowler, C.M.R. & Reston, T.J., 1996. Insight into the nature of the ocean-continent boundary off West Iberia from a deep multichannel seismic reflection profile, *Geology,* **24,** 1079–1082.

Skogseid, J. & Eldholm, O., 1995. Rifted continental margin of mid-Norway, in *Rifted ocean-continent boundaries,* pp. 147–153, eds Banda, E., Talwani, M. & Torne, M. Kluwer Academic Publishers, Netherlands.

Sonder, L. & England, P., 1989. Effects of temperature dependent rheology on large-scale continental extension, *J. geophys. Res.,* **94,** 7603–7619.

Swift, B.A., Sawyer, D.S., Grow, J.A. & Klitgord, K.D., 1987. Subsidence, crustal structure and thermal evolution of Georges Bank basin, *AAPG Bull.,* **71,** 702–718.

Watts, A.B. & Fairhead, J.D., 1997. Gravity anomalies and magmatism along the western continental margin of the British Isles, *J. geol. Soc. Lond.,* **154,** 523–529.

Watts, A.B. & Stewart, J., 1998. Gravity anomalies and segmentation of the continental margin offshore West Africa, *Earth planet. Sci. Lett.,* **156,** 239–252.

Wernicke, B., 1985. Uniform-sense simple shear of the continental lithosphere, *Can. J. Earth Sci.,* **22,** 108–125.

White, N.J., 1994. Recovery of strain-rate variation from inversion of subsidence data, *Nature,* **366,** 449–452.

Whitmarsh, R.B., Manatschal, G. & Minshull, T.A., 2001. Evolution of magma-poor continental margins from rifting to sea-floor spreading, *Nature,* **413,** 150–153.